Progress In Electromagnetics Research C, Vol. 109, 257–273, 2021

Wide Bandwidth Low Profile PIFA Antenna for Vehicular Sub-6 GHz 5G and V2X Wireless Systems

Ahmad Yacoub*, Mohamed Khalifa, and Daniel N. Aloi

Abstract—This paper introduces a low profile wideband Planar Inverted-F antenna (PIFA) for vehicular applications in the 5G systems (below 6 GHz) and Vehicle-to-Everything (V2X) communications. The antenna covers a wide range of bandwidth which operates from 617 MHz to 6 GHz while having an acceptable filtering on the GNSS bands. This design's physical dimensions and electrical performance make it suitable for low profile wireless applications in the automotive field. Measurement data on Ground plane (GND) and on vehicle are presented from a properly cut metal sheet prototype along with simulated results of the model design. Simulation and measurement results are discussed in terms of VSWR, surface current distribution, radiation patterns, antenna efficiency, and linear average gain (LAG).

1. INTRODUCTION

Over the past two decades, the automotive industry has changed drastically. The vehicle's design does not only consist of simple mechanical parts but is now loaded with sensors and wireless systems which has transformed the automobile to a smart device. Recently, the most significant standards that are implemented for vehicle wireless systems are 5G and vehicle-to-everything (V2X) communications via the dedicated short-range communications (DSRC) or the cellular vehicle-to-everything (C-V2X) protocols. These technologies will significantly improve driving experience and have a vital role in developing autonomous vehicles and increase traffic safety. Traffic congestions from and to the cities have increased rapidly due to the high growth of urban areas which has increased the number of car accidents and causes drivers to spend a lot of unnecessary hours on the road which has led to some serious socioeconomic issues. Vehicle-to-X (V2X) communication allows the car's system to communicate with other vehicles, pedestrians, and infrastructures in order to optimize traffic safety, improve self-driving experience, establish connection with Internet of Things (IoT) to different nodes across the network or simply for entertainment systems. 5G network and DSRC are two upcoming technologies that can interwork with each other to provide solutions for V2X communication. The cellular network can be used as a backup to the short-range communication while also providing internet access that can provide information far beyond the DSRC range [1].

The 5G network has an increased frequency band compared to the previous LTE system by adding the frequency band (617 MHz to 698 MHz) and sub-6 GHz bands (3.4 GHz to 5 GHz) in addition to millimeter waves (mmWaves). The system is expected to have data rates up to 10 Gbps at peak, very low latencies up to 1msec, and up to 100 times power consumption efficiency by using smart allocation of RF resources to user nodes [2].

DSRC frequency band in USA is allocated between 5850 MHz and 5925 MHz. The short-range signals improve the vehicle communication with its surroundings and provide various road warnings for traffic safety and public services [3]. The DSRC network as specified by Department of Transportation

Received 6 January 2021, Accepted 5 February 2021, Scheduled 14 February 2021
* Corresponding author: Ahmad Yacoub (ahmadyacoub@oakland.edu).
The authors are with the Electrical and Computer Engineering Department, Oakland University, Rochester hills, MI, USA.

in the USA should be able to operate in a short range of 300 meters (detection range) which can allow spectrum reuse for different nodes and limit the interference between them. It should also have a fast message delivery up to 6 megabytes per second, operates in high speed vehicle scenarios, and is resilient to severe weather conditions such as rain, snow, and fog [4].

The antenna design on vehicles suffers from size limitation and coupling between different elements since usually many applications come in a single package, for instance Cellular, Global Navigation Satellite Systems (GNSS), Satellite Digital Audio Radio Systems (SDARS), and AM/FM in one restricted-size package which raises the issues of antenna size, passive isolation between elements, and bandwidth of each application because the antenna bandwidth depends on the physical volume that it occupies [5, 6].

In this paper, a low profile wideband PIFA antenna has been developed for automotive applications in 5G and DSRC frequency bands. Compared to existing work in literature (summarized in Table 3), the proposed antenna makes it possible to cover B71 band (617 MHz to 698 MHz) with reasonable physical dimensions. This band has been recently freed up by TV broadcasters to be used in 5G applications. The proposed design also has an acceptable rejection for GNSS bands which makes it compatible with different navigation systems. Furthermore, this paper provides data comparison between ground plane and vehicle measurement in terms of different antenna parameters. The antenna in [10] is a novel compact 3D antenna that covers the band from 790 MHz till 2.69 GHz. However, 5G band requires much wider bandwidth that could cover from 617 MHz to 5 GHz. The dimensions of the antennas in [11] and [12] are bigger than the proposed design, and it does not fully cover the desired band from 617 MHz to 5 GHz. The antenna designs from [13] to [18] also cover less frequency bandwidth than the proposed design while also having a larger physical height value.

This paper consists of the following sections. Section 2 describes the design guidelines, proposed antenna geometry, antenna setup on a testing vehicle, and tools used in simulation and measurement. Section 3 presents simulation and measurement results, and comparison to existing designs in literature while also covering the equivalent circuit model for this antenna structure. Section 4 draws conclusions and gives insight to future work.

2. ANTENNA DESIGN LAYOUT

The newly extended 5G band has made it challenging to design a reasonable low-profile antenna specially at the low band where the operating frequencies have shifted lower, and the bandwidth has increased to cover (617 MHz–960 MHz). The conventional monopole would require a radiating height of approximately 95 mm to operate at the center frequency of (788 MHz) which is not practical. A top loaded monopole as presented in [12] can be used to reduce the height to 30 mm at the expense of increasing the length and width dimensions to 80 mm. The proposed design in the paper is derived from a Planar Inverted F-antenna (PIFA) by introducing distinct physical dimensions and slots that would lower its low band operating frequency and increase its bandwidth with smaller occupied volume than those in existing literature. The proposed antenna is made of a metal sheet with dimensions of 28 mm 'height' × 55 mm 'length' × 50 mm 'width', and it is mounted on FR4 board material. The space between the horizontal top plate and the board material is filled with free space (air). Fig. 1 and Fig. 2 show the antenna dimensions from side and top views with its distinct features and variables. The location of the wide feeding plate is placed at the edge of the horizontal plane which is important for the middle and high bands to create folded monopole structures with the slots. A shorting pin is also placed at a specific distance W_d from the feeding plate to control the resonance frequency of the low band. Table 1 shows various geometric parameters of the antenna with their optimized values. The proposed design introduces two new structures containing slot 1 and slot 2 which will create two resonance frequencies at middle and high frequency bands. First, the low frequency band is determined by the physical dimensions of the element in addition to the shorting and feeding pins. Equation (1) approximates the resonance frequency on the low band using the values of Table 1 ($f_c = 790$ MHz) [7]:

$$f_c = \frac{c}{3W + 5.6L + 3.7H - 3W_f - 3.7W_s - 4.3W_d - 2.5L_b} \tag{1}$$

where c is the speed of light ($c = \lambda f$); W, L, and H are width, length, and height of the antenna; W_f is the width of the rectangular feeding plate; W_s is the width of the shorting pin; W_d represents the

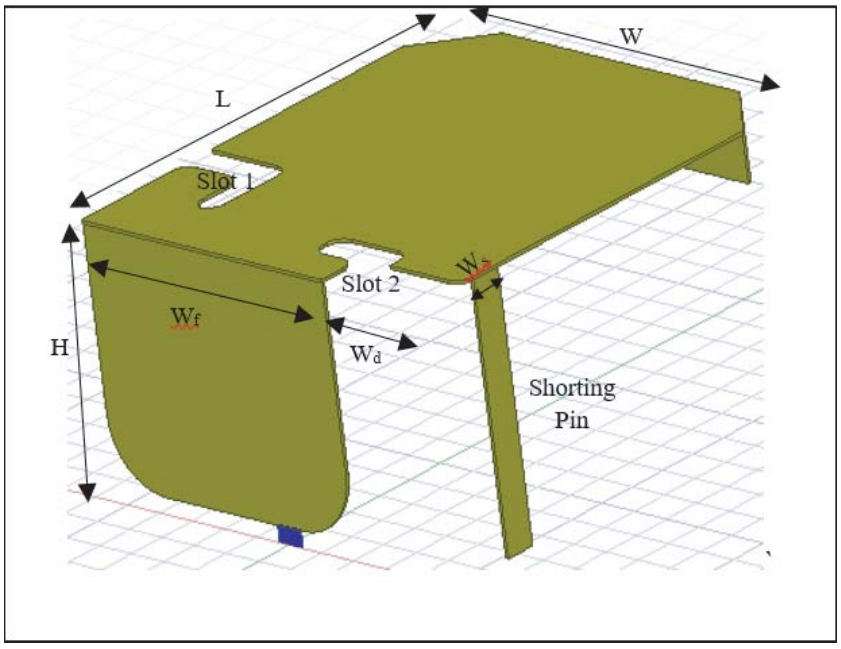

Figure 1. Proposed antenna model with side and front dimensions.

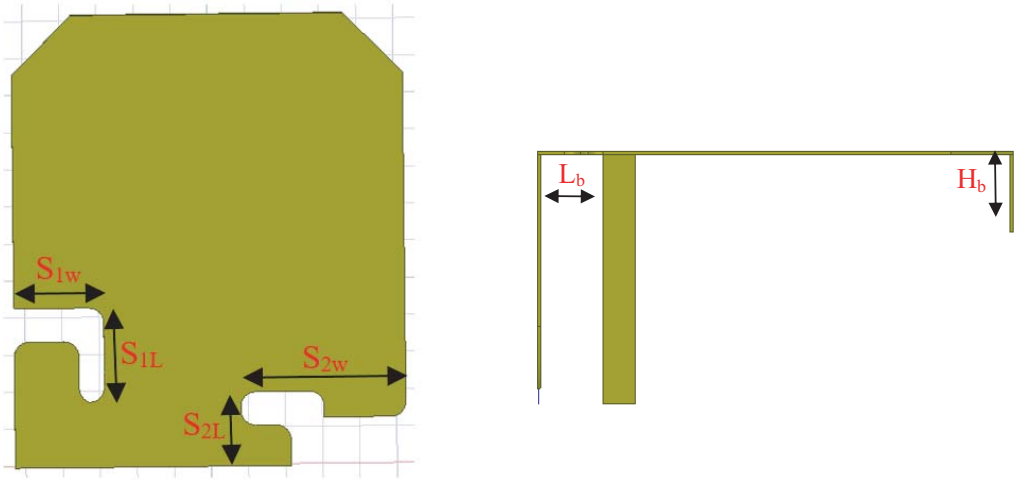

Figure 2. Top and right-side view of the antenna.

width distance between the shorting pin and the rectangular feeding plate; and L_b is the length distance between the shorting pin and the edge of the horizontal top plate. The volume occupied by the antenna determines the bandwidth of the low frequency band which operates from 617 MHz to 960 MHz. The vertical arm of length H_b is added to further reduce the resonance of the low band to around 750 MHz to balance the VSWR values without increasing the total volume.

Secondly, Structure 1 consists of a rectangular feeding plate and up to slot 1. It acts as a folded monopole that has a radiating length of 31.25 mm which is ($\lambda/4$) of 2.39 GHz. The width of the rectangular feeding plate and width of slot 1 determine the bandwidth of the middle band that operates in the frequency range (1.71 GHz–3.8 GHz). Tuning the low band with the proposed element dimensions along with Structure 1 dimensions and gap will filter out the GNSS bands that reside between low and middle cellular frequency bands.

Table 1. Geometrical parameters Values of the designed antenna.

Parameter	Value (mm)	Parameter	Value (mm)
H	28	S_{1L}	12.5
L	55	S_{2w}	22.25
W	50	S_{2L}	10
S_{1w}	12.1	W_f	29.5
W_s	6	H_b	8.5
L_b	7.5	W_d	17.5

Structure 2 consists of a feeding plate and up to slot 2. It acts as a folded monopole with center frequency of 5.5 GHz. Slot 2 changes the current path across the horizontal plane that creates the resonance for the high bands (3.8 GHz–6 GHz). The location of the shorting pin is not only vital for the low frequency band but also important for the DSRC frequencies to avoid getting severe deep nulls (minimum points) in the radiation pattern that will affect the coverage area around the antenna element at the azimuth angles where the shorting pin is located.

Table 2 shows the design goals and performance specifications for this antenna in terms of polarization, return loss, efficiency, and LAG. Many automotive original equipment manufacturers (OEMs) specify 3.3 VSWR for 5G frequencies in the low band range and 2.5 VSWR across 5G high band and V2X bands. They also specify the elevation angles of interest to be theta (75–87 degrees) for 5G systems and theta (80–96 degrees) for V2X.

Table 2. Design goals and requirements.

Parameter	Value
Polarization	Vertical Linear Polarization (VLP)
VSWR	(3.3 VSWR) at 5G bands/(2.5 VSWR) at DSRC band
Efficiency	Minimum 40% at low bands/Minimum 60% at high bands
LAG	-4 dBi across theta (75–87) at 5G/-2 dBi across theta (80–96) at DSRC

The antenna is simulated using HFSS software and measured on a 1-meter rolled edge GND plane inside an anechoic chamber. Then, a vehicle level measurement was conducted with the antenna placed on the back-side center of the roof as shown in Fig. 3. Moreover, semi-analytical methods of treating similar structures to the proposed antenna are presented in the literature [8–13] which are compatible with the simulations and experiments shown in this paper.

3. SIMULATION AND MEASUREMENT RESULTS

The antenna simulated VSWR was captured and compared against the realized antenna measurement as depicted in Fig. 4. It is noticed that across the operating bands of 5G and DSRC, the measured VSWR is better than 3.3 : 1 (approximately -5.4 dB return loss). The VSWR plot also shows a reasonable rejection for GNSS frequencies.

The vector surface current distribution of the antenna measured in (A/m) is plotted in Fig. 5. At each frequency, the intensity and direction of the current distribution are presented along the entire structure. It can be noticed that the low frequency bands present the most intense current in the structure specially at the feeding plate and shorting pin where the direction of current is in-phase between them, while going up in the frequency range the surface current starts shifting towards slot 1 structure for frequencies up to 3.8 GHz. Fig. 5 also shows that at the high end of 5G frequencies and DSRC, the current shifts from slot 1 towards slot 2 structure. Fig. 6(a) shows the equivalent circuit model

Figure 3. Antenna Placement on vehicle roof.

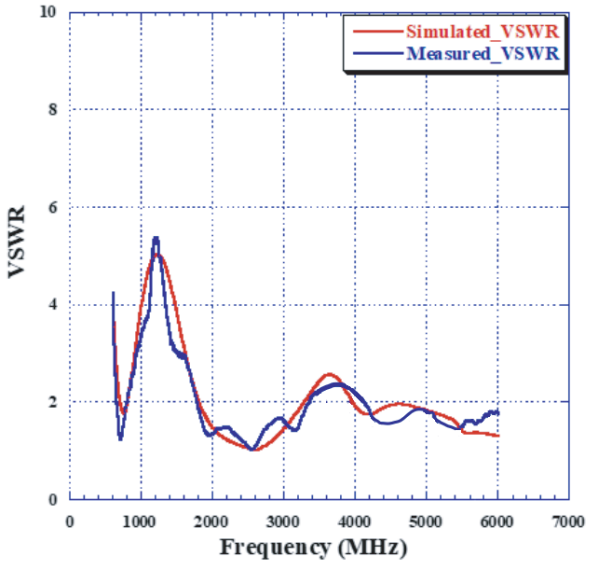

Figure 4. On GND simulated and measured VSWR.

for this wideband PIFA antenna. The method of designing this circuit is presented in [14] derived from the VSWR response. Fig. 6(b) shows the response of the circuit model using ADS software compared with the simulated VSWR of the antenna. The circuit consists of multiple RLC resonance circuits which simulate low, mid, and high frequency resonances in addition to GNSS filtering as presented by the vector current distribution on the PIFA.

In Fig. 7, radiation patterns of horizontal cuts at elevation 80 degrees are presented for frequencies 617 MHz, 1.9 GHz, 3.6 GHz, and 5 GHz. It can be concluded that for low frequencies the patterns tend to have a good omnidirectional behavior; however for higher frequencies, radiation patterns appear more directive. At 3.6 GHz, it seems directive towards the side of slot 1 while at 5 GHz it appears directive at slot 2 angles from the front and back sides of the element. Moreover, the average gain observed from vehicle radiation patterns is found to be -2.1 dBi, -1 dBi, 0 dBi, and 0.9 dBi at frequencies 617 MHz, 1.9 GHz, 3.6 GHz, and 5 GHz, respectively.

It is important for DSRC radiation patterns to avoid having extreme minimum values (nulls) as it will influence the coverage range at certain azimuth angles. Fig. 8 shows the radiation pattern for

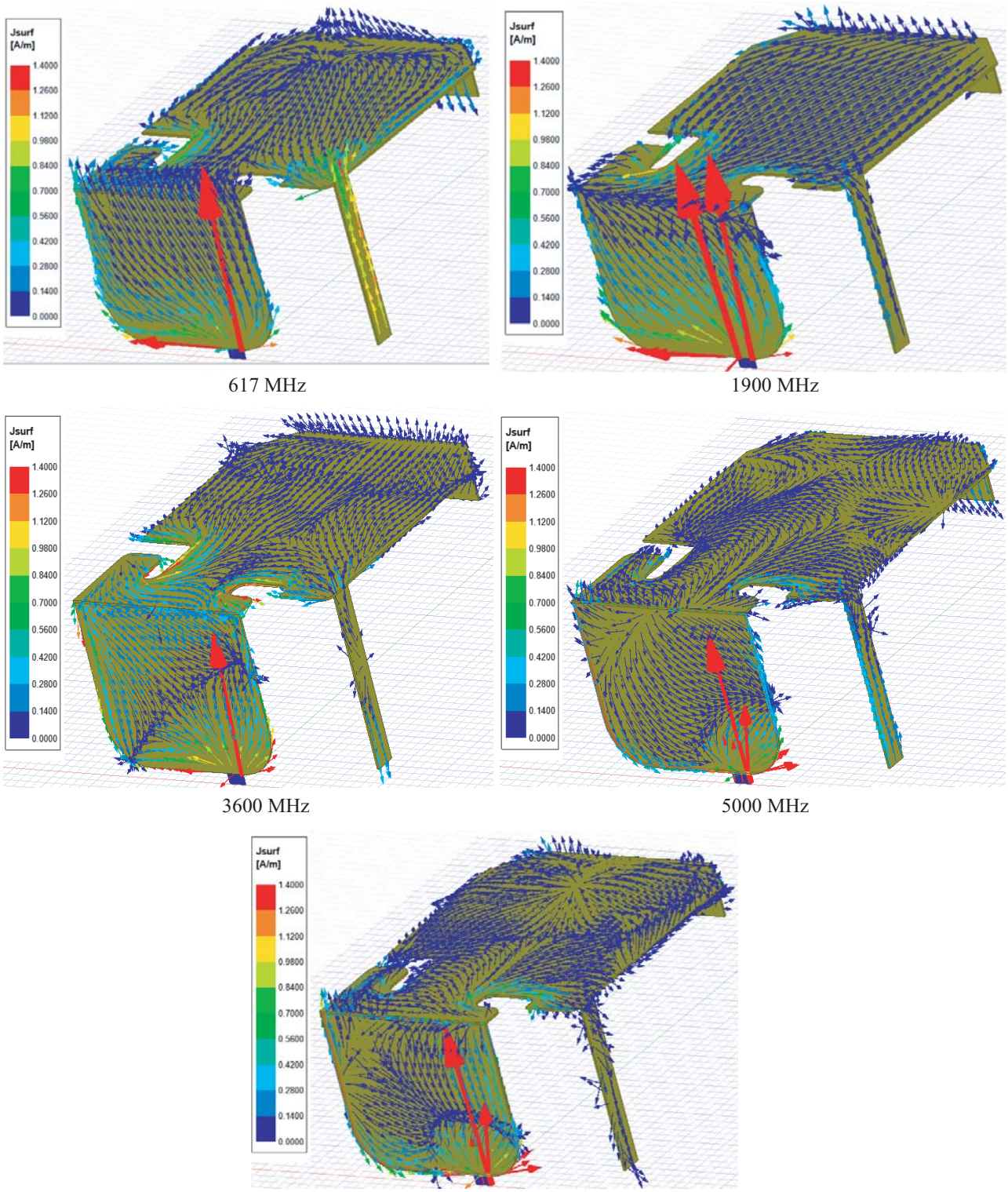

Figure 5. Simulated vector surface current distribution measured in (A/m) at different 5G and DSRC frequencies.

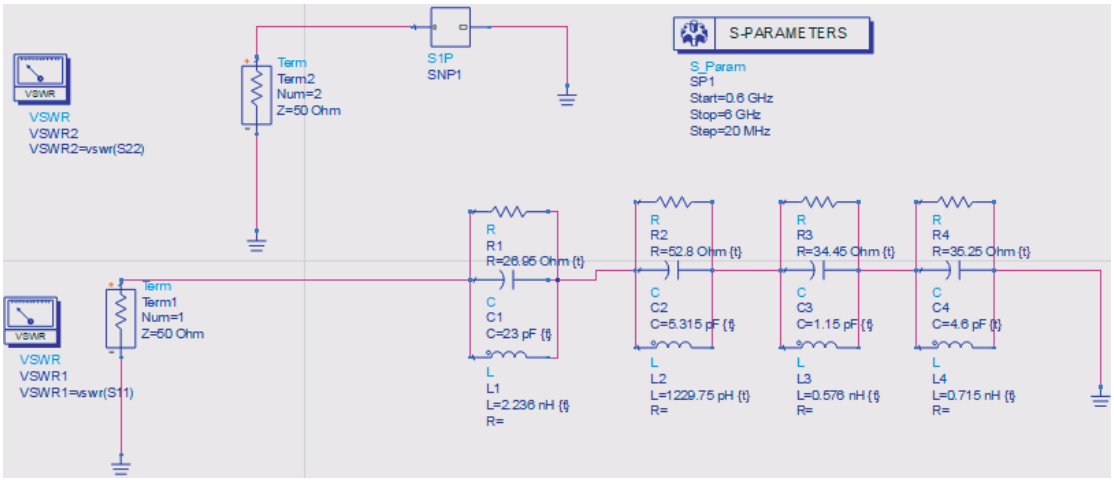

(a)

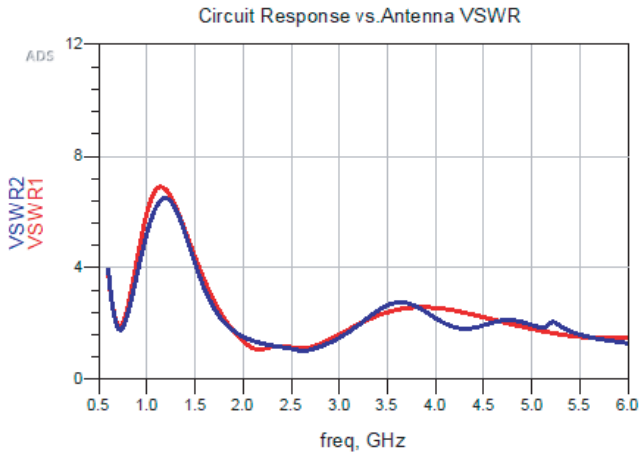

(b)

Figure 6. Equivalent lumped elements circuit model using ADS and comparison between the circuit response and antenna's VSWR. (a) Equivalent electrical circuit model of the antenna. (b) Circuit response vs. antenna VSWR.

5.9 GHz frequency measured on GND and on vehicle at elevation 90 degrees. The vehicle radiation pattern tends to be more directive towards the back side of the car which could result from reflections caused by the roof's curvature with a peak gain of 4.4 dBi at azimuth angle 230 degrees without having a minimum value lower than −12 dBi.

The measured antenna efficiencies on GND and vehicle for 5G bands have been presented in Figs. 9(a), (b), and (c). It can be noticed that the 5G GND measurement has an average of 83% efficiency across all frequency bands whereas the vehicle measurement has a reduced average efficiency of 72% that could result from reflections of EM waves from the roof curvature and paint which worsens the grounding of the antenna specially at the low frequency bands.

The measured antenna efficiency for DSRC frequencies is shown in Fig. 9(d). The GND and vehicle efficiencies seem to have close values across the band. This could be reasoned by the size of the ground surrounding the antenna since at these high frequencies the area of the ground plane can be reduced without having major losses unlike the cases at lower frequency bands. The measured GND efficiency has an average of 71% across the band while the measurement on vehicle has an average of 69%.

The LAG for 5G frequencies is calculated across the elevation angles 3 to 15 degrees above the horizon. These angles mimic the incoming RF signals incident from cellular towers. Figs. 10(a), (b),

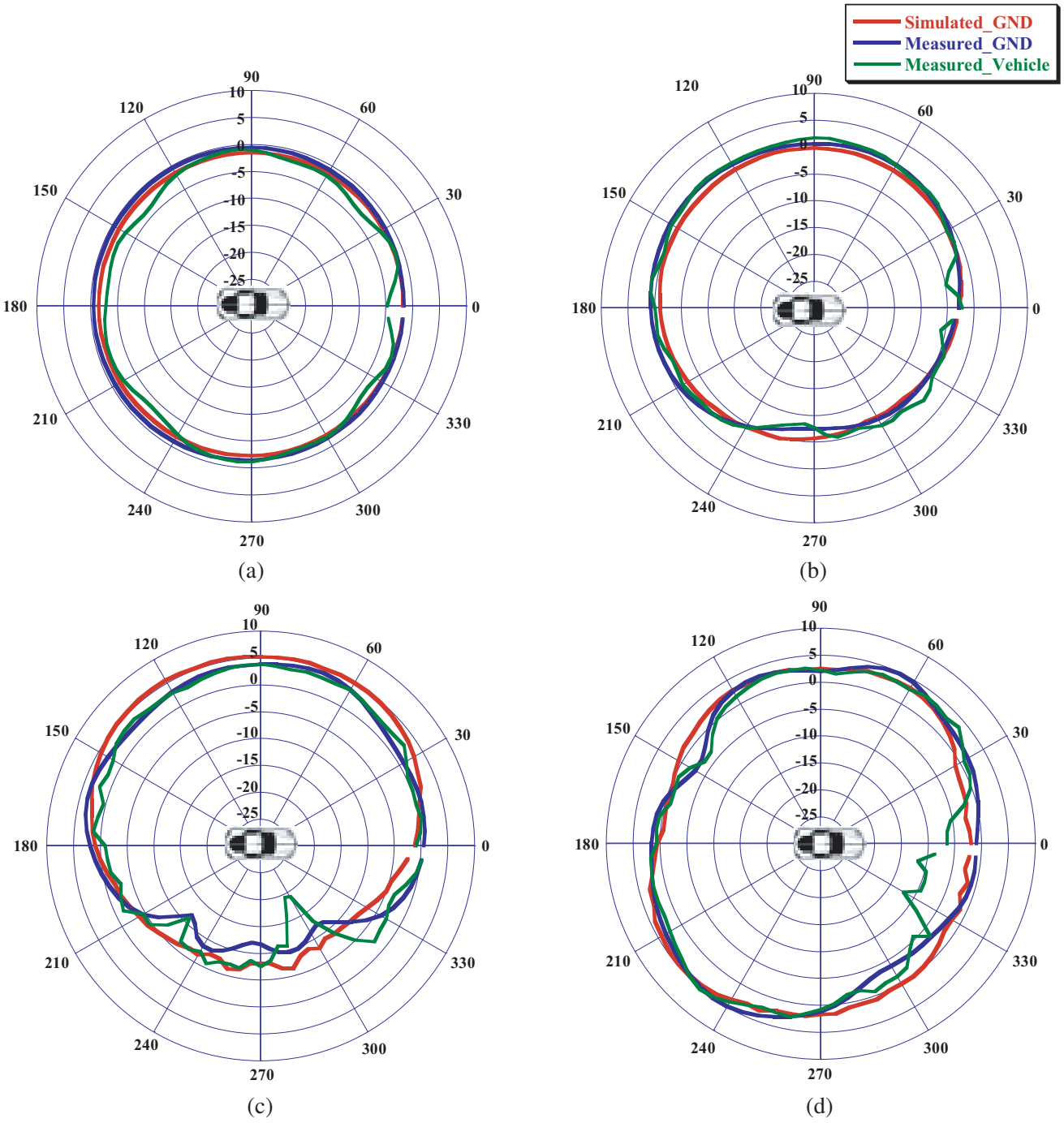

Figure 7. Radiation pattern of simulated, measured on GND, and measured on vehicle gain in (dBi) at 80 deg. of elevation at frequencies: (a) 617 MHz, (b) 1900 MHz, (c) 3600 MHz, and (d) 5000 MHz.

and (c) show the LAG measured across all frequency bands from 75 to 87 degrees of theta. In general, vehicle LAG is slightly lower than GND LAG; however, both measurements perform better than −2 dBi across the entire band with most of the frequency range measuring positive values which indicate a good antenna performance.

Figure 11 shows the LAG measured for DSRC frequencies across elevation angles 80 to 96 degrees. The vehicle's LAG is slightly better in this case than the GND LAG, and this results from below the horizon angles (91–96 degrees). The ground plane at these angles is blocking the signal path to the

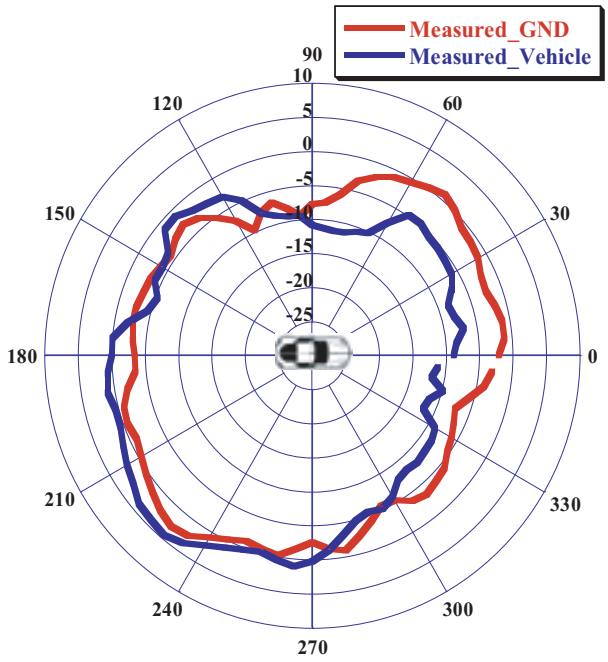

Figure 8. Gain in (dBi) Radiation pattern measured on GND and on vehicle at 90 deg. of elevation at 5.9 GHz frequency.

antenna, while on vehicle this effect is less because of the vehicle's roof and curvature. However, it can be noted that in both measurements, the LAG values are better than −0.87 dBi across all frequency points.

Next, the parametric study of significant geometrical parameters and features in the antenna design is presented using simulation. In reference to Fig. 1 and Fig. 2, the parameters that are investigated include: 1) Height of element H, 2) Length of the element L, 3) Width of the element W, 4) Width of

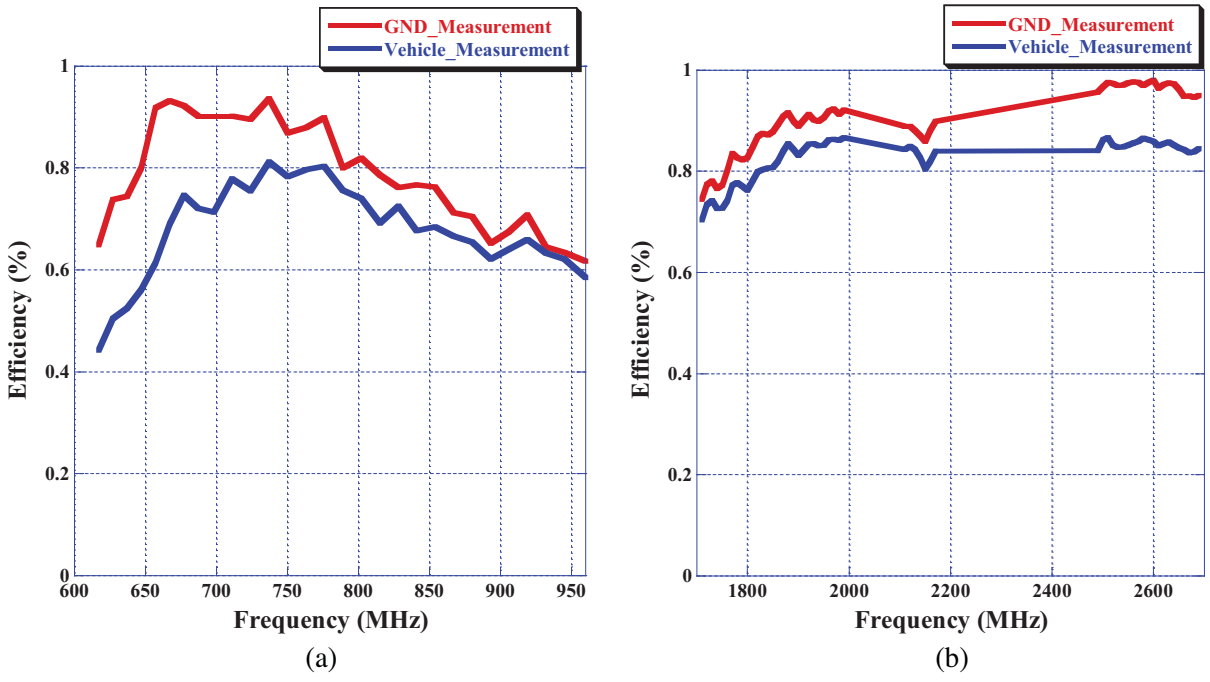

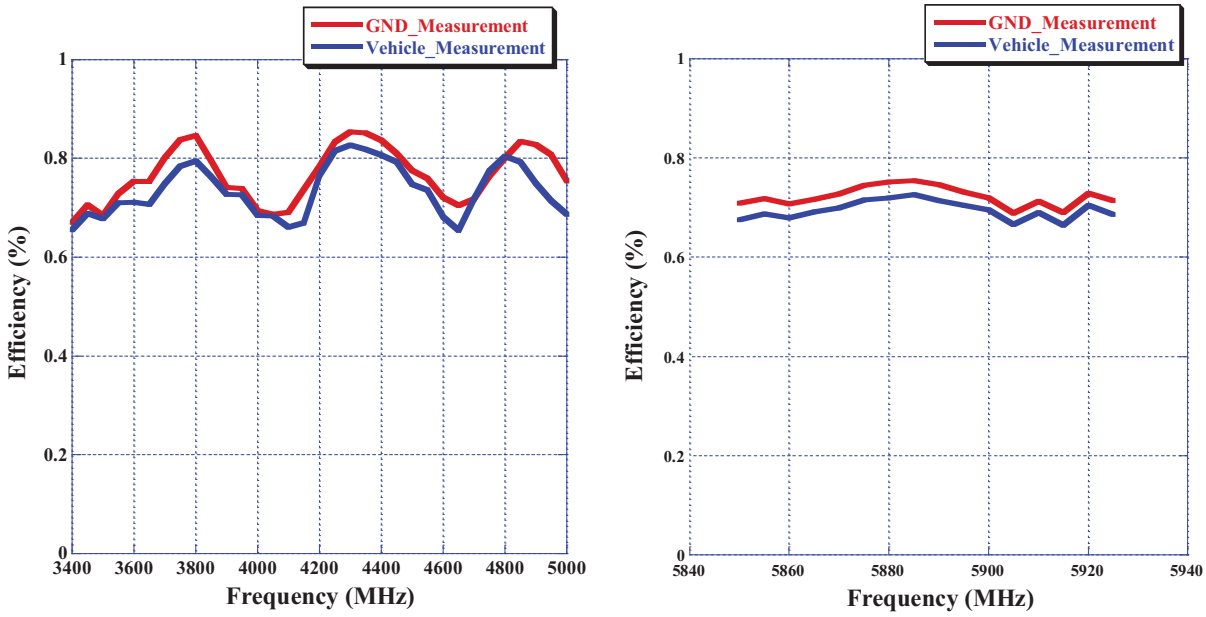

Figure 9. Antenna efficiency measured on ground plane and on vehicle for 5G and DSRC frequencies: (a) 617 MHz–960 MHz, (b) 1710 MHz–2690 MHz, (c) 3400 MHz–5000 MHz, (d) 5850 MHz–5925 MHz.

the rectangular feeding plate W_f, 5) Width of the shorting pin W_s, 6) Length and width of slot 1 (S_{1L}, S_{1w}), 7) Length and width of slot 2 (S_{2L}, S_{2w}).

Figure 12 shows the variation of VSWR for three different values of H including 23 mm, 28 mm, and 33 mm. It can be noticed that parameter H influences low and high frequency bands. This is because decreasing height H will reduce the volume of the antenna, and hence operating bandwidth is less especially in the low band region. Also, reducing the height will tune the antenna towards higher frequencies for both low and high frequency bands as can be seen in Fig. 12. Choosing the value 28 mm for H is optimal to meet the size limitation requirement with acceptable RF performance.

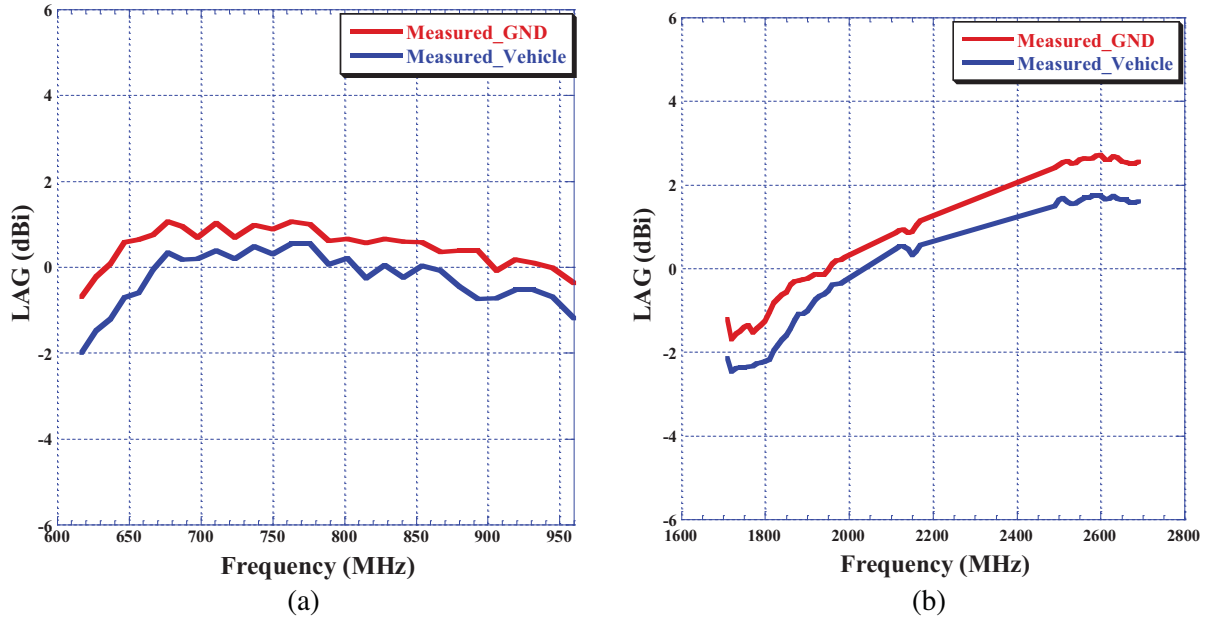

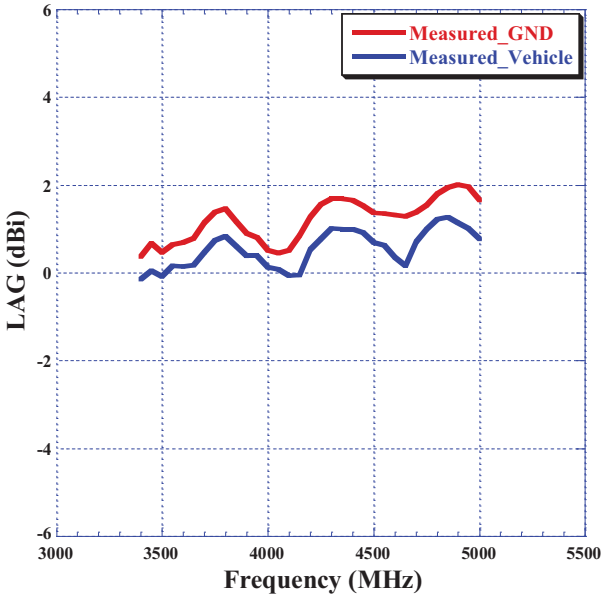

(c)

Figure 10. Measured LAG in (dBi) on GND and on vehicle for 5G frequencies from theta equals 75 to 87 degrees: (a) 617 MHz–960 MHz, (b) 1710 MHz–2690 MHz, (c) 3400 MHz–5000 MHz.

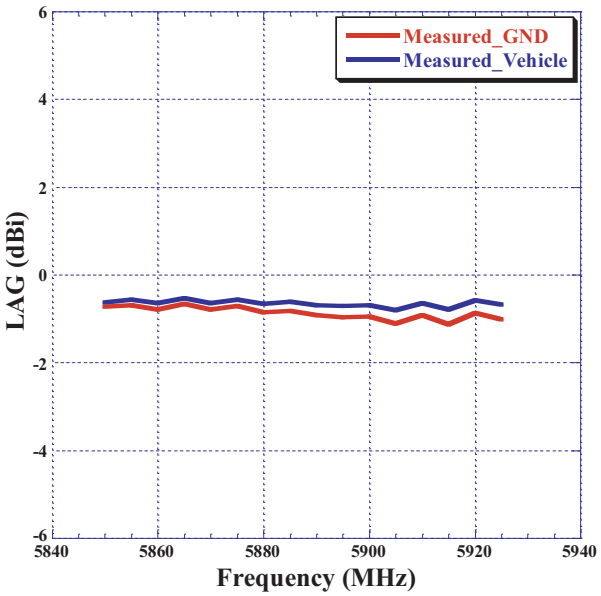

Figure 11. Measured LAG in (dBi) on GND and on vehicle for DSRC frequencies from theta equals 80 to 96 degrees.

Furthermore, changing the value of parameter L has a significant role in the low frequency bands. As shown in Fig. 13, increasing the value of L will support a bigger wavelength current in the low frequency band which will improve VSWR at 617 MHz at the expense of higher VSWR at 960 MHz.

In Fig. 14, the width of the element W is analyzed for three different values: 40 mm, 50 mm, and 60 mm. The parameter W has a significant effect across the entire operating bands since the location of the shorting pin changes. It can be concluded that reducing the width of the element will reduce

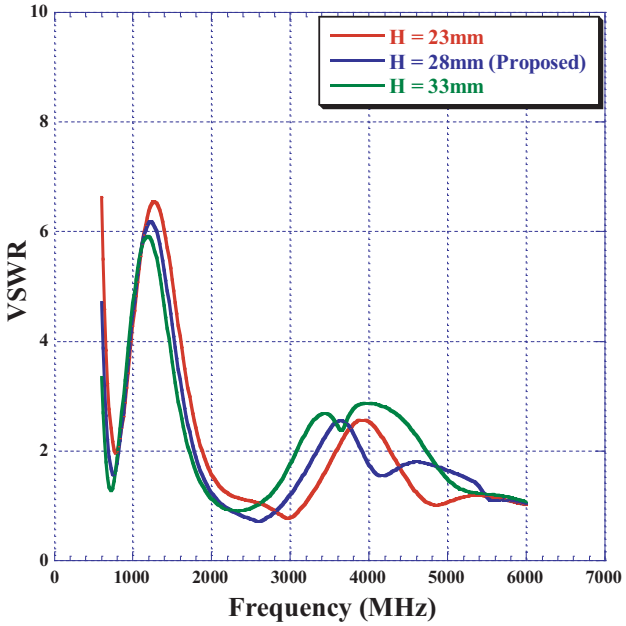

Figure 12. VSWR of varying the height of the element H.

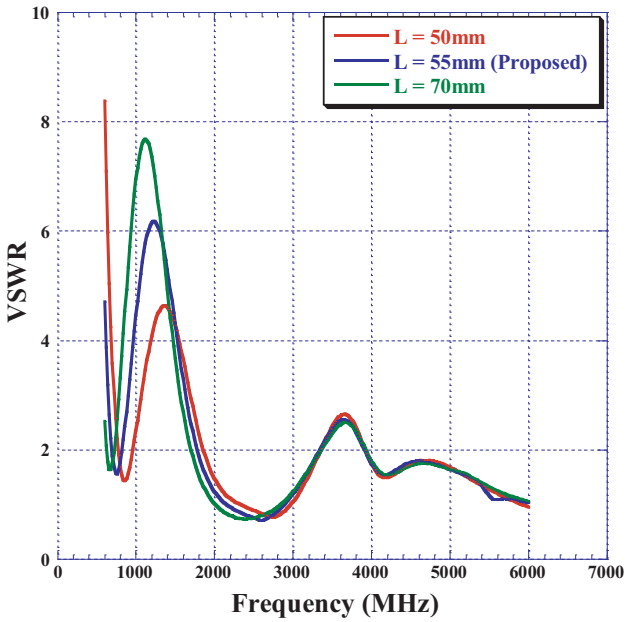

Figure 13. VSWR of varying the length of the element L.

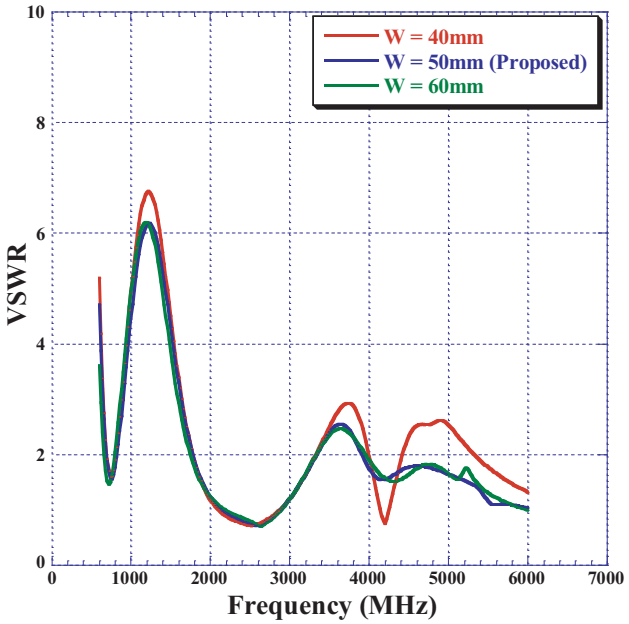

Figure 14. VSWR of varying the width of the element W.

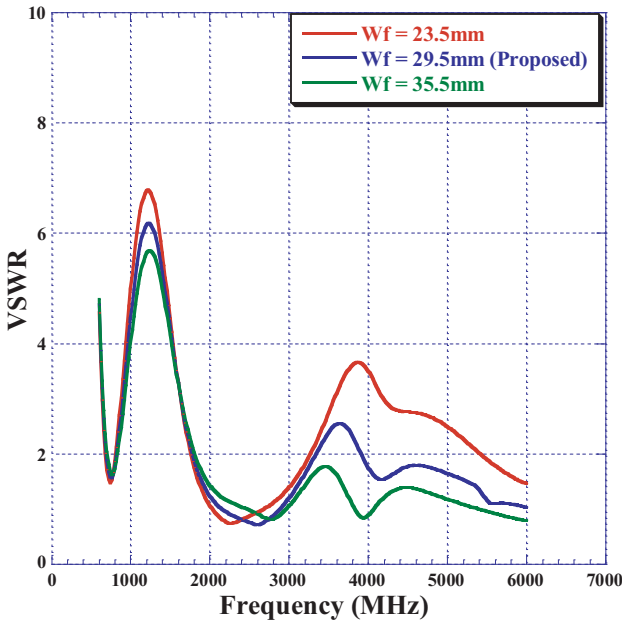

Figure 15. VSWR of varying the width of the feeding plate W_f.

the volume of the antenna structure and hence decreases the bandwidth specially at the low band (617 MHz–960 MHz). Reducing W also influences the VSWR at the high band since the shorting pin gets closer to slot 2. It can be found that a value of 50 mm as proposed in this antenna is optimal for performance and physical size.

The width of the rectangular feeding plate W_f has a role in slightly changing the resonance frequency in the low band as calculated in Equation (1). It also has an important role in specifying the bandwidth

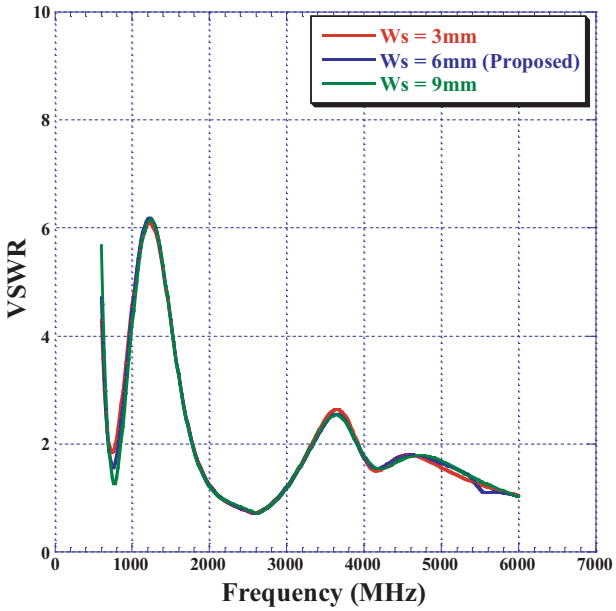

(a) 617 MHz-6 GHz

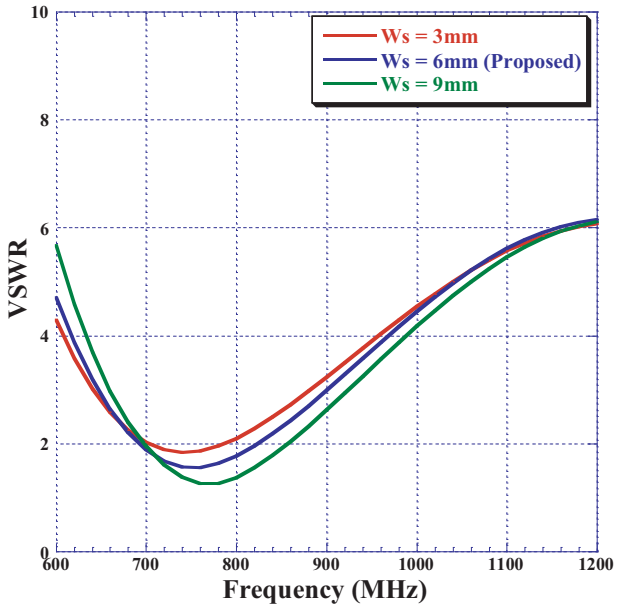

(b) 617 MHz-960 MHz

Figure 16. VSWR of varying the width of the feeding plate W_s: (a) across low and high band, (b) across low frequency band (617 MHz–960 MHz).

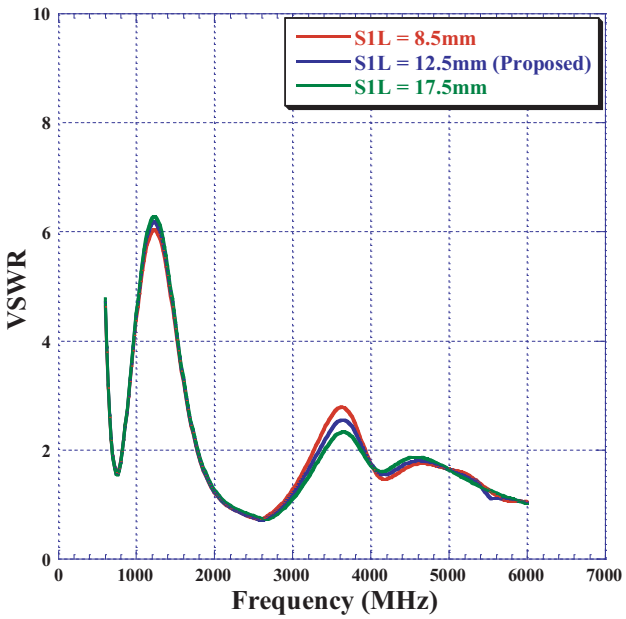

Figure 17. VSWR of varying slot 1 length S_{1L}.

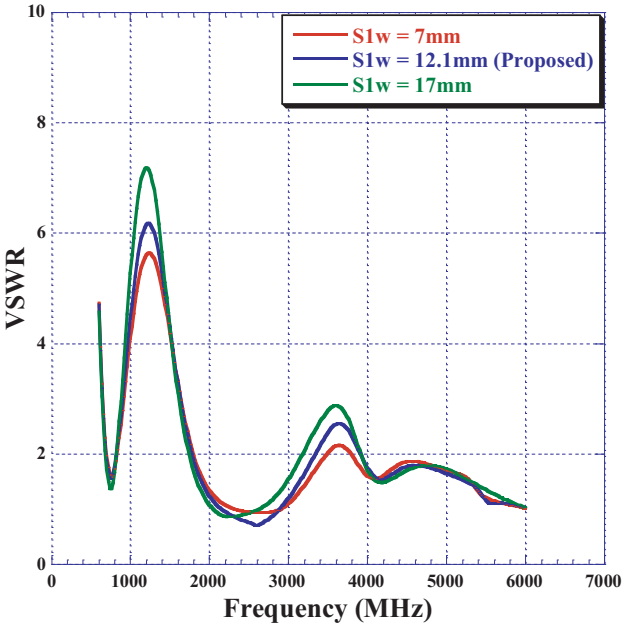

Figure 18. VSWR of varying slot 1 width S_{1w}.

of the higher bands as shown in Fig. 15. Reducing the width of the feeding plate tunes the antenna lower in frequency and reduces the operating bandwidth across the whole range. Hence, choosing W_f to be 29.5 mm is suitable for antenna impedance and physical width of the element.

Figure 16 shows the effect of changing the width of the shorting pin W_s. Equation (1) shows that W_s influences the resonance frequency of the low band. As shown in Fig. 16, changing the width of the shorting pin among 3 mm, 6 mm, and 9 mm does not have a major effect on the high bands, but it shifts the resonance frequency in the low band. In Fig. 16(b), it can be noticed that increasing the width of

the shorting pin tunes the antenna higher in frequency. Hence, choosing W_s to be 6 mm is optimal to balance the VSWR across low band frequency range.

To study the effect of changing the length and width of slot 1, S_{1L} and S_{1w}, one parameter is changed at a time while the other one remains at its proposed value. It is observed from Fig. 17 and Fig. 18 that varying these parameters will have their most effect on the VSWR in the high frequency band. So, choosing S_{1L} and S_{1w} to be 28 mm and 11 mm respectively will balance the VSWR across

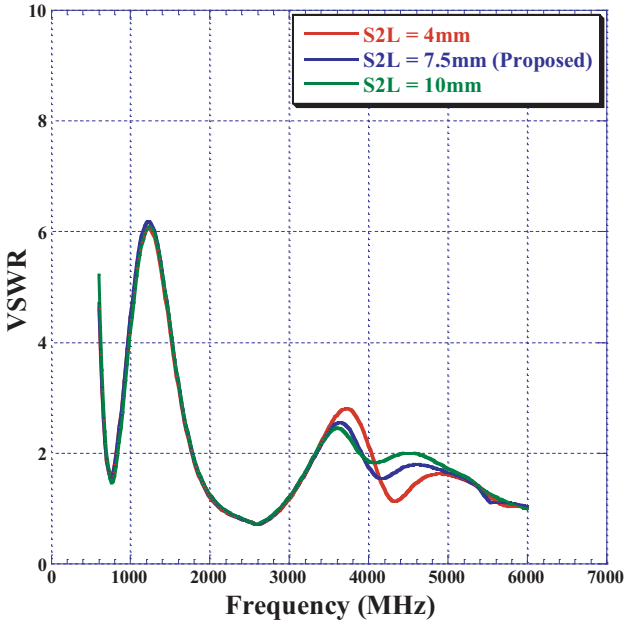

Figure 19. VSWR of varying slot 2 length S_{2L}.

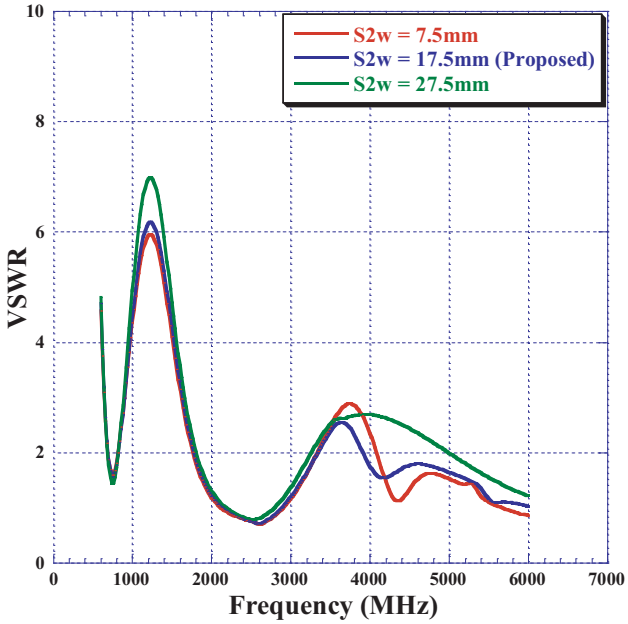

Figure 20. VSWR of varying slot 2 length S_{2w}.

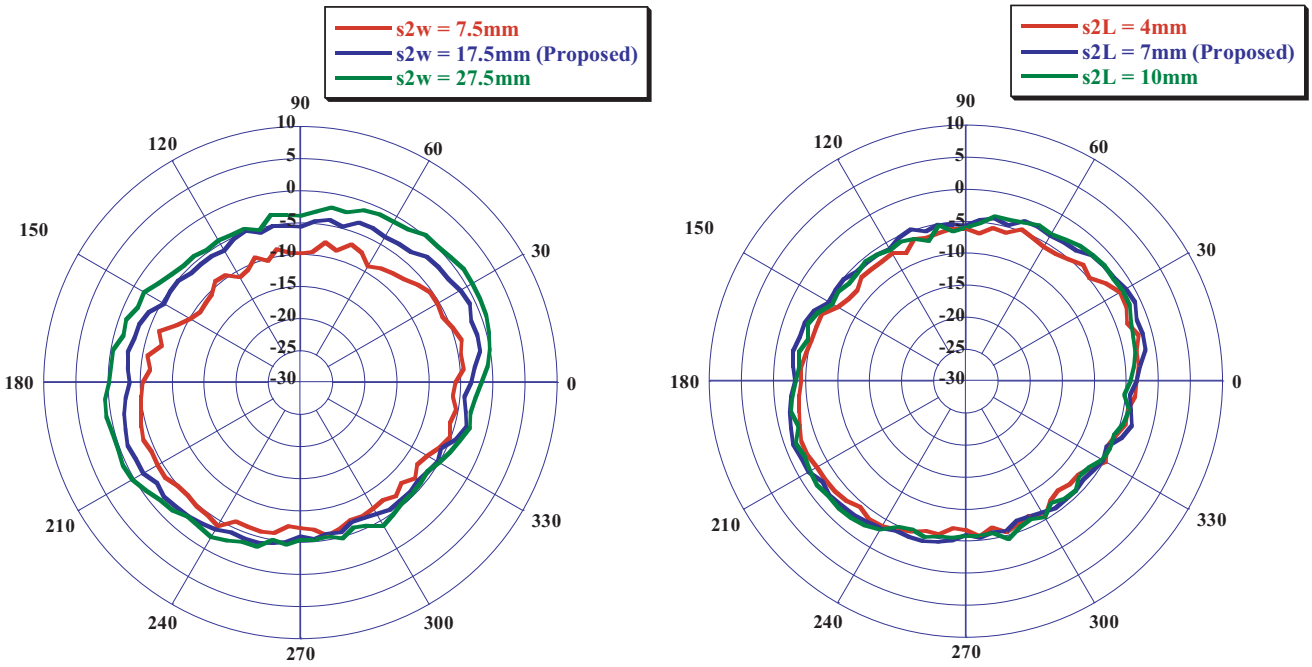

Figure 21. DSRC radiation pattern at 5.9 GHz varying slot 2 dimensions.

the middle frequency bands.

Figures 19 and 20 show the effect of changing the width and length of slot 2 on the VSWR. With reference to Equation (1), slot 2 dimensions control the distance between the feeding plate and the shorting pin, so they influence the low band resonance frequency. Fig. 19 and Fig. 20 also show the effect on the 5G high frequency and V2X bands as the shorting pin location changes with slot 2 dimensions. Fig. 21 shows the effect of parameter varying of slot 2 on the DSRC gain pattern. It can be concluded that reducing the dimensions of slot 2 will introduce more losses going through the shorting pin since the current will have a faster path to ground. Therefore, choosing slot 2 parameters

Table 3. Comparison between proposed antenna and literature.

	Type	**Bandwidth**	**Dimensions ($\mathbf{L \times W \times H}$) ($\mathbf{mm^3}$)**	**Gain/ Efficiency**
Proposed Antenna	Compact PIFA	617 MHz–6 GHz	$55 \times 50 \times 28$	Average gain on vehicle −2.1 dBi @617 MHz, −1 dBi @1.9 GHz, 0 dBi @3.6 GHz and 0.9 dBi @5 GHz. Average efficiency 83% on GND, 72% on Vehicle.
15	Novel compact 3D antenna	790 MHz–2.69 GHz	$50 \times 50 \times 30$	Simulated Max. gain 1–2.5 dB at low band, 6–8.5 dB at higher bands.
16	Nefer Antenna	698 MHz–6 GHz	$80 \times 60 \times 30$	−3 dB (High band gain is in driving direction) (70% 0.7–3.7 GHz, 63% 3.7–6 GHz on GND)
17	Top-loaded monopole	700 MHz–3 GHz	$80 \times 80 \times 28$	Average gain on GND −2 dBi @752 MHz, −1.5 dBi @892 MHz, −2 dBi @1.755 GHz and −1.5 dBi @1.93 GHz. (73.3% @752 MHz, 76.4% @892 MHz, 85% @1.755 GHz, 95.3% @1.93 GHz)
18	Printed monopole	698 MHz–2690 MHz	$25 \times 1.53 \times 76$	Measured gains are higher than 2 dB
19	Vivaldi monopole	698 MHz–4 GHz	$69.1 \times 0.86 \times 73$	Max gain/efficiency: 3.64 dBi/97.83% @700 MHz, 3.54 dBi/91.29% @900 MHz 5.21 dBi/89.28% @1.8 GHz 5.54 dBi/80.58% @2.1 GHz 6.42 dBi/85.43% @2.5 GHz)
20	T-Shape monopole	698 MHz–960 MHz 1.427 GHz–2.7 GHz	$33 \times 10 \times 55$	Max gain 2.8 dBi @900 MHz, 5.2 dBi @2.6 GHz. Average efficiency 70%.
21	3-port printed antenna	0.69 GHz–0.96 GHz 1.7 GHz–2.7 GHz/ (2.4 GHz/5 GHz)/ DSRC (5.9 GHz)	$87 \times 1.6 \times 60$	Gain at 2.4 GHz varies from −10 to 2.4 dBi. Average gain @0.69 GHz −1 dBi/0.96 GHz −3 dBi/1.7 GHz −2 dBi/2.7 GHz −5 dBi Max gain at 5.9 GHz is 2 dBi to the front and −0.5 dBi to the back.
22	Printed PICA	800 MHz–10 GHz	$76.2 \times 0.79 \times 76.2$	Max gain: 4 dBi @1 GHz 6 dBi @5 GHz 8 dBi @9 GHz
23	Printed annular monopole	0.69 GHz–10 GHz	$140 \times 1.524 \times 86$	Gain from 0.6 dBi to max of 4.2 dBi

as proposed will balance the VSWR curve and have a reasonable radiation pattern at DSRC frequencies.

Table 3 shows a comparison between different cellular antenna designs that already exist in the literature and how the proposed antenna in this paper has improvements on frequency bandwidth, dimensions, and performance.

4. CONCLUSION

A low-profile wideband antenna has been presented in this paper which functions across 5G frequency band from 617 MHz to 5 GHz and across DSRC band from 5850 MHz to 5925 MHz. It consists of a wide rectangular plate at the feeding pin with two cut slots to control high frequency bands and a shorting pin for low frequency band. The antenna is simulated using HFSS simulation tool and then measured on a 1-meter GND and on a testing vehicle inside an anechoic chamber. The measurements show a VSWR better than (3.3 : 1) and an average efficiency of 83% on a GND and 72% on the vehicle for 5G frequencies while DSRC frequencies has an average efficiency of 71% on GND and 69% on vehicle. In general, the proposed antenna design is a good candidate for low-profile antenna applications on vehicle. Future work will be focused on developing a 5G/V2X MIMO system that will provide diversity, increased capacity, and higher throughput.

ACKNOWLEDGMENT

The authors would like to acknowledge Oakland University for providing measurements facilities and simulation tools.

REFERENCES

1. Abboud, K., H. A. Omar, and W. Zhuang, "Interworking of DSRC and cellular network technologies for V2X communications: A survey," *IEEE Transactions on Vehicular Technology*, Vol. 65, No. 12, 9457–9470, Dec. 2016.
2. Wang, C., J. Bian, J. Sun, W. Zhang, and M. Zhang, "A survey of 5G channel measurements and models," *IEEE Communications Surveys & Tutorials*, Vol. 20, No. 4, 3142–3168, Fourth quarter 2018.
3. Ghafari, E., A. Fuchs, D. Eblenkamp, and D. N. Aloi, "A vehicular rooftop, shark-fin, multiband antenna for the GPS/LTE/cellular/DSRC systems," *2014 IEEE-APS Topical Conference on Antennas and Propagation in Wireless Communications (APWC)*, 237–240, Palm Beach, 2014.
4. https://www.its.dot.gov/research_archives/connected_vehicle/pdf/DSRCReportCongress_FINAL_23NOV2015.pdf.
5. Arianos, S., G. Dassano, F. Vipiana, and M. Orefice, "Design of multi-frequency compact antennas for automotive communications," *IEEE Transactions on Antennas and Propagation*, Vol. 60, No. 12, 5604–5612, Dec. 2012.
6. Artner, G., W. Kotterman, G. Del Galdo, and M. A. Hein, "Automotive antenna roof for cooperative connected driving," *IEEE Access*, Vol. 7, 20083–20090, 2019.
7. Chattha, H., Y. Huang, X. Zhu, and Y. Lu, "An empirical equation for predicting the resonant frequency of planar inverted-F antennas," *Antennas and Wireless Propagation Letters*, Vol. 8, 856–860, IEEE, 10.1109/LAWP.2009.2027822, 2009.
8. Yang, L., N. Liu, Z. Zhang, G. Fu, Q. Liu, and S.-L. Zuo, "A novel single feed omnidirectional circularly polarized antenna with wide AR bandwidth," *Progress In Electromagnetics Research C*, Vol. 51, 35–43, 2014.
9. Valagiannopoulos, C., "Single-series solution to the radiation of loop antenna in the presence of a conducting sphere," *Progress In Electromagnetics Research*, Vol. 71, 277-294, 2007.
10. Narbudowicz, A., X. L. Bao, and M. J. Ammann, "Dual-band omnidirectional circularly polarized antenna," *IEEE Transactions on Antennas and Propagation*, Vol. 61, No. 1, 77–83, Jan. 2013.

11. Fikioris, G. and C. Valagiannopoulos, "Input admittances arising from explicit solutions to integral equations for infinite-length dipole antennas," *Progress In Electromagnetics Research*, Vol. 55, 285–306, 2005.
12. Chen, L., X. Ren, Y.-Z. Yin, and Z. Wang, "Broadband CPW-fed circularly polarized antenna with an irregular slot for 2.45 GHz RFID reader," *Progress In Electromagnetics Research Letters*, Vol. 41, 77–86, 2013.
13. Valagiannopoulos, C., "An overview of the Watson transformation presented through a simple example," *Progress In Electromagnetics Research*, Vol. 75, 137–152, 2007.
14. Sayidmarie, K. and L. Yahya, "Modeling of dual-band crescent-shape monopole antenna for WLAN applications," *International Journal of Electromagnetics and Applications*, Vol. 4, 31–39, doi:10.5923/j.ijea.20140402.01, 2014.
15. Franchina, A. M., P. Nepa, R. Parolari, I. Moro, A. Polo Filisan, and D. Zamberlan, "A 3D LTE antenna for vehicular applications," *IEEE International Symposium on Antennas and Propagation & USNC/URSI National Radio Science Meeting*, 637–638, San Diego, CA, Jul. 2017
16. Hastürkoğlu, S. and S. Lindenmeier, "A wideband automotive antenna for actual and future mobile communication 5G/LTE/WLAN with low profile," *11th European Conference on Antennas and Propagation (EUCAP)*, 602–605, Paris, Mar. 2017.
17. Ghafari, E. and D. N. Aloi, "Top-loaded UWB monopole antenna for automotive applications," *Proceedings of the 2012 IEEE International Symposium on Antennas and Propagation*, 1–2, Chicago, IL, Jul. 2012.
18. Michel, A., P. Nepa, M. Gallo, I. Moro, A. Polo Filisan, and D. Zamberlan, "Printed wideband antenna for LTE-band automotive applications," *IEEE Antennas and Wireless Propagation Letters*, Vol. 16, 1245–1248, Nov. 2016.
19. Navarro-Méndez, D. V., et al., "Compact wideband vivaldi monopole for LTE mobile communications," *IEEE Antennas and Wireless Propagation Letters*, Vol. 14, 1068–1071, 2015.
20. Goncharova, I. and S. Lindenmeier, "A high efficient automotive roof-antenna concept for LTE, DAB-L, GNSS and SDARS with low mutual coupling," *2013 9th European Conference on Antennas and Propagation (EuCAP)*, 1–5, Lisbon, Apr. 2015.
21. Hua, Y., L. Huang, and Y. Lu, "A compact 3-port multiband antenna for V2X communication," *2017 IEEE International Symposium on Antennas and Propagation & USNC/URSI National Radio Science Meeting*, 639–640, San Diego, CA, 2017.
22. Suh, S.-Y., W. L. Stutzman, and W. A. Davis, "A new ultrawideband printed monopole antenna: the Planar Inverted Cone Antenna (PICA)," *IEEE Transactions on Antennas and Propagation*, Vol. 52, No. 5, 1361–1364, May 2004.
23. Liang, X., S. Zhong, W. Wang, and F. Yao, "Printed annular monopole antenna for ultra-wideband applications," *Electronics Letters*, Vol. 42, No. 2, 71–72, Jan. 19, 2006.